

Detection of Epithelial-Cell Injury, and Quantification of Infection, in the HCT-8 Organoid Model of Cryptosporidiosis

Cirle Alcantara Warren,¹ Raul V. Destura,^{1,3} Jesus Emmanuel A. D. Sevilleja,^{1,3} Luis F. Barroso,¹ Humberto Carvalho,² Leah J. Barrett,¹ Alison D. O'Brien,² and Richard L. Guerrant,¹

¹Center for Global Health, University of Virginia, Charlottesville; ²Uniformed Services University of the Health Sciences, Bethesda, Maryland;

³National Institutes of Health-University of the Philippines, Manila

Background. Intestinal cells grown in microgravity produce a three-dimensional tissue assembly, or “organoid,” similar to the human intestinal mucosa, making it an ideal model for enteric infections such as cryptosporidiosis.

Methods. HCT-8 cells were grown in a reduced-gravity, low-shear, rotating-wall vessel (RWV) and were infected with *Cryptosporidium parvum* oocysts. Routine and electron microscopy (EM), immunolabeling with fluorescein-labeled Vicia villosa lectin and phycoerythrin-labeled monoclonal antibody to a 15-kD surface-membrane protein, and quantitative polymerase chain reaction (qPCR) using probes for 18S rRNA of *C. parvum* and HCT-8 cells were performed.

Results. The RWV allowed development of columnar epithelium-like structures. Higher magnification revealed well-developed brush borders at the apical side of the tissue. Incubation with *C. parvum* resulted in patchy disruption of the epithelium and, at the surface of several epithelial cells, in localized infection with the organism. EM revealed irregular stunting of microvilli, foci of indistinct tight junctions, and areas of loose paracellular spaces. qPCR showed a 1.85-log (i.e., 70-fold) progression of infection from 6 h to 48 h of incubation.

Conclusion. The HCT-8 organoid displayed morphologic changes indicative of successful and quantifiable infection with *C. parvum*. The HCT-8 organoid–culture system may have application in interventional in vitro studies of cryptosporidiosis.

In vitro and in vivo models of cryptosporidial infection have been limited by both the lack of close approximation to the human intestinal environment and variability in physiologic responses to the pathogen. Molecular pathogenesis in cryptosporidiosis has been extensively studied in cell monolayers [1–3], as well as in a limited number of animal models, such as piglets, calves, and

neonatal or immunodeficient mice [4–8]. However, there is always the question of whether these current models of infection are physiologically relevant to infection in humans. Furthermore, results of interventional studies in vitro may be drastically different, and available animal models are cumbersome and, again, may not be representative of what actually occurs in humans in vivo. Although studies using human volunteers are ideal, the ethical issues involved and the low infectious dose for *Cryptosporidium* species, which may be harmful to the unsuspecting immunocompromised hosts, further limit experimental studies in humans.

An alternative to current models of infection is the use of the low-shear modeled microgravity–analogue culture system, which produces a three-dimensional tissue assembly, or “organoid.” It has been observed by US National Aeronautics and Space Agency scientists that cell lines grown during space flight tend to develop native tissue-like structures [9]. The low-shear microgravity environment can be simulated in the laboratory by use of a bioreactor or a rotating-wall vessel (RWV) that

Received 14 August 2007; accepted 28 December 2007; electronically published 22 May 2008.

Potential conflicts of interest: none reported.

Presented in part: 44th annual meeting of the Infectious Disease Society of America, Toronto, Canada, 00–00 October 2006 (abstract 352).

Financial support: Middle Atlantic Regional Center of Excellence for Biodefense and Emerging Infectious Diseases Research (grant U54 AI057168 to C.A.W. and R.L.G.); International Training on Emerging Infectious Diseases (grant 45 D45 TW00909 to R.V.D. and J.E.A.D.S.); Ellison Medical Foundation and Pfizer Initiative in Health at University of Virginia (support to J.E.A.D.S.).

Reprints or correspondence: Dr. Cirle Alcantara Warren, Div. of Infectious Diseases and International Health, University of Virginia, Charlottesville, VA 22901 (ca6t@virginia.edu).

The Journal of Infectious Diseases 2008; 198:143–9

© 2008 by the Infectious Diseases Society of America. All rights reserved.

0022-1899/2008/19801-0023\$15.00

DOI: 10.1093/infdis/jin143

keep cells in suspension during culture. This system subjects the cells to a time-averaged gravitational field (vector-averaged gravity), to simulate low-gravity conditions, in which spatial co-location among and assembly of individual cells into large aggregates can occur [10]. Small- and large-intestinal cell lines that have been cultured in this condition have shown cellular polarity, apical brush borders, intercellular junctions, and basal lamina [11, 12]. More recently, an HCT-8 cell line grown in bioreactors has been shown to form organoids with microvilli and desmosomes characteristic of normal tissue [13]. Furthermore, the staining patterns of cytokeratin, E-cadherin, simplekin, and villin have been noted to be more similar to those in human intestinal epithelium in tissue assemblages grown in bioreactors than to those in cell monolayers grown in culture plates.

Few bacterial pathogens have been studied in cells grown in bioreactors; as of the writing of the present article, the only published studies are of *Salmonella enterica* serovar Typhimurium in Int-407 and HT-29 cells, *Pseudomonas aeruginosa* in A549 lung epithelial cells, and enteropathogenic and enterohemorrhagic *Escherichia coli* in HCT-8 cells [13–16]. In the present study, we report the first application of the low-shear microgravity culture system for a category B parasite, *C. parvum*. We describe the development of the HCT-8 organoid model of cryptosporidiosis, the effects that infection has on epithelial cells, and the quantification of infection.

METHODS

Excystation of *C. parvum*. Commercially available (Waterborne) *C. parvum* oocysts suspended in PBS were subjected to 20% bleach (final volume) for 10 min and were centrifuged at 402 g for 5 min, and all but 100 μ L of the supernatant was discarded. Hanks' balanced salt solution (HBSS) (Cambrex) was then added to neutralize the bleach. The mixture was thoroughly blended by vortexing and was centrifuged at 402 g for another 5 min, and all but 100 μ L of the supernatant was discarded. These steps were done 4 or 5 times, until the HBSS did not change color. The pellet was then resuspended in HCT-8 medium prior to infection. A hemocytometer was used to estimate the excystation rate, by counting the number of oocysts before and after the procedure; the difference between the 2 counts was considered to be the number of oocysts that had excysted.

Organoid culture system. Human colonic adenocarcinoma (HCT-8) cells (American Type Culture Collection) were cultured in 75-cm² flasks containing RPMI medium supplemented with 10% horse serum and 100 IU of penicillin-streptomycin. The cells were grown in an incubator with CO₂ at 37°C and were passed by enzymatic dissociation via Accutase (Chemicon). The low-shear microgravity environment was attained by using a rotary cell-culture (RCC) system, an RWV, or a bioreactor (Synthecon). The bioreactor was housed in a humidified incubator with 5% CO₂ at 37°C. Dehydrated porcine small-intestinal sub-

mucosa grafts (Cook Biotech) (size, 2 × 3 mm) were placed in a 50-mL RCC disposable vessel filled with culture medium (RPMI medium supplemented with 10% horse serum and Pen/Strep). After 2–4 h of preincubation, the RCC vessel was seeded with 10⁵ HCT-8 cells/mL. The initial rotation of the vessel was set at 10 rpm, and the speed was adjusted as the cell aggregates grew. The medium was changed after 3 days and every 4 days thereafter. Bubbles in the vessels were aspirated as necessary. After 8 days of incubation, one set ($n = 4$) of the organoids was transferred to another rotating vessel and was inoculated with excysted *C. parvum* oocysts (Waterborne) at a concentration of 10⁵/mL. Another set ($n = 4$) was transferred to another vessel and served as a control. All organoids initially were incubated for 6 h, to allow excysted *C. parvum* to infect the HCT-8 cells in the infected vessels. The medium was then changed again. After 24 h of incubation, the organoids were harvested for examination.

To quantify infection rates, another set of organoids was inoculated with excysted *C. parvum* 8 days after incubation. For comparison, HCT-8 monolayers (80%–90% confluent) in culture plates also were infected with *C. parvum*. The medium was replaced after 6 h, and the HCT-8 cells were reincubated and harvested at 2, 6, 12, 24, and 48 h postinfection. In another set of experiments, intended to quantify infection rates over an extended period of time, organoids (4 per time point) were harvested at 0, 24, 48, 72 and 96 h postinfection. A corresponding set of uninfected organoids (4 per time point) was harvested to serve as a control. In this setup, 10-mL RCC vessels were seeded with either HCT-8 or *C. parvum* oocysts, at the same concentrations as noted above.

Light microscopy. After being harvested, all organoids were transferred to tissue cassettes and were fixed in 4% paraformaldehyde. After 2 h, they were immersed in 70% ethanol until being embedded in paraffin blocks for the purpose of thin sectioning. Organoid thin sections were stained with hematoxylin-eosin and Giemsa and were examined under low-, high-, and oil immersion-power magnification. Some slides were left unstained, for immunolabeling.

Immunolabeling. Unstained sections were deparaffinized by 2 successive 5-min washings in xylene. The sections were then immersed, for 2–5 min at each concentration, in decreasing concentrations—100%, 95%, and 75%—of ethanol and were rinsed in deionized water. Then they were incubated in 0.1% Triton X-100 for 20 min and were blocked with 1% bovine serum albumin for 30 min. A monoclonal antibody against the 15-kD membrane protein of intracellular *C. parvum* (Biodesign International) was labeled with phycoerythrin, according to the manufacturer's instructions (Zenon rabbit IgG labeling kit; Invitrogen), and then was placed on the slides containing the organoid sections. After 60 min, the slide was washed with PBS and was incubated in fluorescein-labeled Vicia villosa lectin (Vector Laboratories) specific to *C. parvum* sporozoites. After fixation in

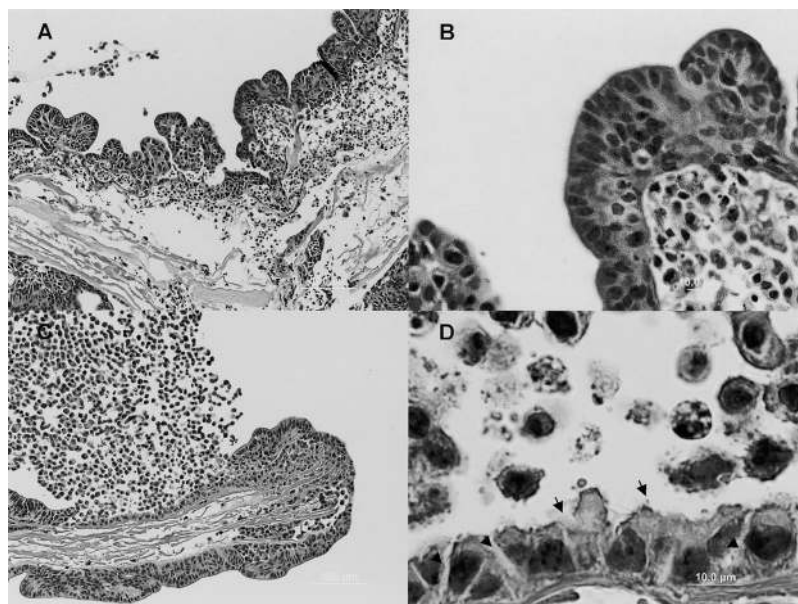


Figure 1. A, Low-power microscopy of HCT-8 cells organoid showing villus-like epithelial folds around the bioscaffold. At high-power magnification, the HCT-8 cells formed layers of cells, with the outermost layer showing polarization of cells and development of apical brush borders. B, Loosely organized undifferentiated HCT-8 cells underneath the HCT-8 cell layers. C, Infected organoid showing localized infection and detachment of both uninfected and infected cells in the affected area. D, Oil immersion–power magnification showing disruption of apical brush borders (arrows) and looseness of intercellular attachments (arrowheads). In the vicinity were several detached cells, including possibly apoptotic cells.

4% paraformaldehyde, the stained organoid slides were examined by epifluorescent microscopy.

Electron microscopy. For electron microscopy, uninfected and infected organoids were transferred to tissue cassettes and were fixed in 4% paraformaldehyde and 2.5% glutaraldehyde in 0.1 mol/L phosphate buffer (pH 7.3–7.4). Further processing was performed at the Advanced Microscopy Section of the University of Virginia. Postfixation was performed with 1% osmium tetroxide, for 1 h. The samples then were dehydrated with acetone and were infiltrated with epoxy resin. When infiltration with 100% epoxy resin was complete, the samples were baked at 60°C for 48 h, to harden them. Sections (0.5 μ m and 60 nm) were cut by use of a Leica Ultracut E ultramicrotome and were examined by use of a JEOL 1230 transmission electron microscope.

Real-time polymerase chain reaction (PCR). DNA was extracted from infected and uninfected HCT-8 cells and from pure *C. parvum* oocysts, according to the supplier's recommended procedure (DNeasy Tissue Kit; Qiagen). Organoids were harvested and were placed in an Eppendorf tube containing 100 μ L of Accutase, to which 20 μ L of proteinase K, followed by 200 μ L of buffer AL, was then added. After the contents of the tube had been mixed, it was placed in a 70°C water bath for 10 min. Then 200 μ L of 100% ethanol was added, and the mixture was filtered at 8000 rpm for 1 min. The filter was then washed twice with buffer, first at 8000 rpm for 1 min and then at 14,000 rpm for 3 min. Recovery of the DNA was performed with 200 μ L of elution buffer, by centrifugation at 8000 rpm for 1 min. Quan-

tification of infection was performed by real-time PCR (BioRad iCycler; Hercules) using primers for the 18s rRNA gene of *C. parvum* (Cp18SR931 [5'-CTGCGAATGGCTCATTATAACA-3']; GenBank accession number X64341) and the 18s rRNA gene of HCT-8 cells (i.e., the housekeeping gene) [5'-GGTTCGAA-GACGATCAGA-3']; GenBank accession NR_003286), as described elsewhere [17]. For every sample, the reaction mixture was composed of 12.5 μ L of BioRad iQ SYBR Green Supermix, 5.5 μ L of Fisher nuclease-free water, and 1 μ L each of the forward and reverse primers. Two reaction mixtures were prepared, one for detection of *C. parvum* and the other for detection of HCT-8 cells. A 20- μ L portion of the reaction mixture was placed at the bottom of the wells of a 96-well PCR plate. A 5- μ L sample of DNA was then added to each well. Amplification consisted of 15 min at 95°C, followed by 40 cycles of 15 s at 95°C, 30 s at 60°C, and 30 s at 70°C. Amplification and detection were performed by use of the iCycler real-time detection system (Bio-Rad). Fluorescence was measured during the annealing step of each cycle. The cycle number of each run was compared to a standard curve of known amounts of *Cryptosporidium* DNA and was converted into parasite count per HCT-8 cell.

RESULTS

The HCT-8 organoid. Incubation of HCT-8 cells in RWV allowed development of stratified cuboidal-to-columnar epithelium-like structures around the bioscaffold (figure 1). In some areas, the epithelium folded and formed villus-like

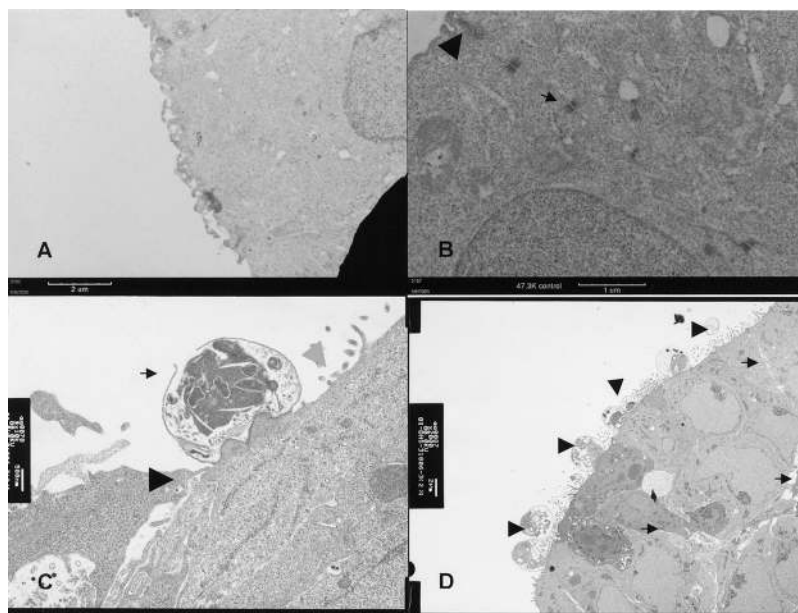


Figure 2. A and B, Electron micrographs of uninfected organoids showing (A) well-developed microvilli and distinct junctional apparatuses, including tight junctions (arrowhead), and (B) desmosomes (arrow). C, Infected organoids with a meront (arrow), probably in the process of releasing merozoites, indistinct tight junctions (black arrowhead), and denudation of the apical surface (gray arrowhead). D, Area of multiple infection with *Cryptosporidium parvum* at different stages of development (arrowheads) and loosening of the paracellular spaces (arrows). Notably, the tight junctions and desmosomes became inapparent in the infected organoids.

structures with loose cells underneath the organized layer of cell aggregates. The outermost layer of cells showed polarization, with the nuclei tending to be basally oriented. At higher magnification, these cells revealed well-developed brush borders at the apical side of the tissue. Electron microscopy showed well-developed microvilli, tight junctions, and other intercellular junctional apparatus (figure 2).

C. parvum–infected HCT-8 organoids. Incubation with *C. parvum* resulted in patchy disruption of the epithelium, interrupted by areas of intact epithelium (figure 1). At the surface of several epithelial cells there was localized infection with trophozoites. Some infected and uninfected cells were observed to be detached from the affected epithelium. Immunolabeling confirmed intracellular localization of *C. parvum* in infected cells (figure 3). Light microscopy and immunolabeling also revealed the organism at different stages of its life cycle. Parasitophorous vacuoles were revealed by electron microscopy (figure 2). Transmission electron micrography also revealed irregular stunting of microvilli, which was seen even in some uninfected adjacent cells. In contrast to what was observed in uninfected controls, there were foci of indistinct tight junctions, as well as areas of loose paracellular spaces, in infected organoids. Junctional apparatus such as desmosomes and zona adherens were inapparent in most organoid sections.

Quantification of infection. The excystation rates of *C. parvum* used in these experiments were ~30%–35%. The inocula of oocysts were incubated in the RCC vessels for 6 h, to allow excysted oocysts to attach to and infect the HCT-8 cells. Unat-

tached sporozoites were removed by changing the medium. Using pure oocysts as a standard and the HCT-8 cell housekeeping gene, real-time PCR showed that the progression of infection from 6 h to 48 h of incubation was 1.85 logs (70-fold) in the organoids but only 1.04 logs (i.e., 10.7-fold) in the monolayers. However, the infection rates were higher in the monolayers than in the organoids: at 6, 12, 24, and 48 h postinfection, the respective infection rates were 0.040, 0.266, 0.498, and 2.848 in the organoids, compared with 0.464, 0.351, 1.072, and 4.977 in the monolayers (figure 4A–C). Peak infection appeared to occur at 48 h during the extended period of incubation (the initial parasite count was 22 at 0 h and had increased to 247 by 48 h). Interestingly, infection decreased to the baseline value by 72 h and to 0 by 96 h, possibly because of apoptosis of infected HCT-8 cells and detachment of even viable cells during infection. PCR of supernatant at 96 h revealed 933 detectable *C. parvum*, suggesting continued viability of the organism but release to the surrounding medium because of friability and cell death occurring in the infected organoids. Uninfected organoids had HCT-8 cell counts of 1.9×10^5 at 0 h, 8×10^5 at 24 h, 2.3×10^5 at 48 h, and 2×10^5 at 96 h. No cryptosporidial DNA was detected in uninfected organoids.

DISCUSSION

In the present study, the development of HCT-8 organoids by use of the RCC system was successfully replicated and, to our knowledge, was applied for the first time to protozoal infection.

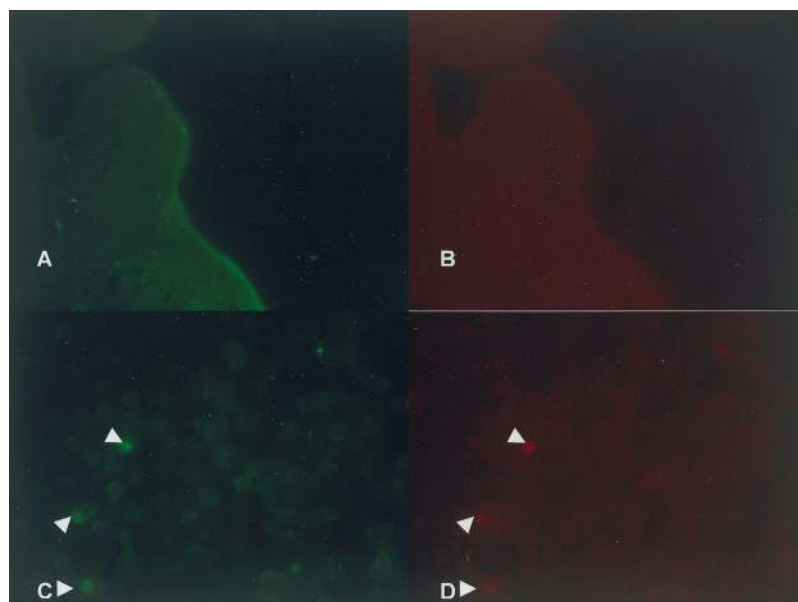


Figure 3. Fluorescent imaging of infected and uninfected HCT-8 cells. *A* and *B*, Uninfected cells stained with fluorescein-labeled *Vicia villosa* lectin specific to intracellular *Cryptosporidium parvum* sporozoites and to phycoerythrin-labeled monoclonal antibody against the 15-kD membrane protein of *C. parvum*, respectively. *C* and *D*, Intracellular *C. parvum*-positive cells (arrowheads) in infected organoids.

HCT-8 cells formed layers of cells, with the outermost layer being similar to the intestinal epithelium in humans and clearly showing well-developed microvilli and intercellular junctions. It has been reported elsewhere that villin, a cytoskeletal protein of

the intestinal epithelial microvilli, is expressed predominantly on the apical surface of the organoids, a finding that is consistent with what has been observed in normal human small intestine [13]. Furthermore, compared with those in cell monolayers, the

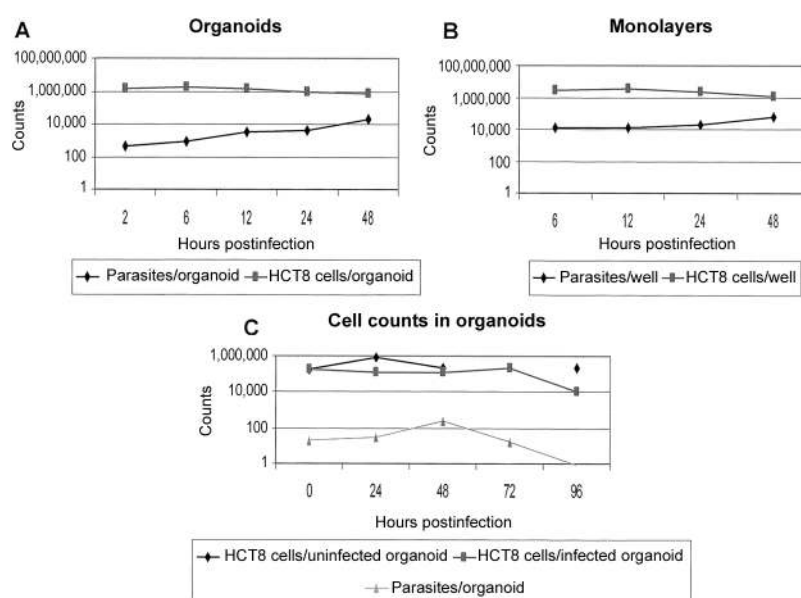


Figure 4. Comparison of infection rates for HCT-8 organoids vs. those for monolayers, by use of quantitative polymerase chain-reaction with *Cryptosporidium parvum* and HCT-8 cell probes. The organoids showed a steady increase in infection from 6 h to 48 h. The infection rates were higher in monolayers (*B*) than in organoids (*A*), but the rate of increase was more pronounced in the organoids than in the monolayers. In extended incubation, after the peak of infection at 48 h, there is a steady decrease in parasite burden, starting 76 h postinfection (*C*). In contrast to the more stable number of cells in the intact, uninfected organoids, the number of HCT-8 cells decreases at 96 h, suggesting that, in infected organoids, there is cell detachment from the bioscaffold.

staining patterns of tight-junction proteins, E-cadherin, ZO-1, and simplekin in organoids have been shown to be more similar to those in normal human tissue. These findings suggest that the HCT-8 organoid may be an ideal model for cryptosporidiosis, a parasitic infection that causes both malabsorption and increased intestinal permeability [1, 18, 19]. Indeed, the *C. parvum*-infected organoids showed blunting of microvilli and disruption of tight junctions, a finding consistent with what has been described in biopsy specimens from infected patients [20–22].

Although there was no attempt to quantify the degree of epithelial-cell injury, the infection rate was measured by real-time PCR using pure oocysts and the HCT-8 housekeeping gene for standardization. The use of the housekeeping gene was critical, because both organoids and monolayers have variable amounts of host cells. The proportion of infected cells in the organoids was lower than that in the monolayers, but the rate of increase of infection in the organoids was higher and more persistent than that in the monolayers. This finding may be consistent with what has been observed in three-dimensional assemblages of Int-407 cells and HT-29 cells infected with *Salmonella* Typhimurium, a situation in which invasion has been noted to be decreased [15, 16]. Similarly, *P. aeruginosa* has been observed to attach to and to penetrate three-dimensional aggregates of A549 lung epithelial cells significantly less efficiently than it penetrates monolayers, and this has been attributed to the enhanced formation of tight-junction complexes [14]. These observations may suggest that a higher degree of cellular differentiation in the organoids offers greater resistance to invading pathogens.

The ability both to identify epithelial injury—in terms of denuded microvilli and junctional apparatus abnormalities—and to quantify infection opens the possibility of applying this model to preventive and therapeutic interventional studies. We hypothesize that the physiologic response to drugs, vaccines, and micronutrients that is observed in this model may be more akin to the human intestinal-cell response in vivo, because, as discussed above, the RCC system leads to the development of features more similar to those in human tissue. Indeed, primary cell lines cultivated in the condition of simulated microgravity maintain key metabolic functions and probably respond to pathogens in the same manner as they do in vivo [23, 24]. Moreover, the low-shear low-turbulence environment of microgravity-analogue culturing is similar to that found in certain in vivo conditions, such as those in utero and in the protected environment between the brush border microvilli of epithelial cells in humans [25–28]. The latter environment is relevant to that encountered by microbial pathogens and commensals during their life cycles in the gastrointestinal, respiratory, and urogenital tracts. In this setting, the pathogen's response during infection—a response that includes gene expression, physiology, and pathogenesis—seems to be affected by these mechanical forces [29–32]. Whether these findings

could be generalized to all bacteria or to other pathogens—for example, protozoa such as *Cryptosporidium*—warrants further investigation.

In conclusion, we have successfully developed an organoid model of cryptosporidial infection. The HCT-8 organoid has been found to display morphologic changes indicative of successful and quantifiable infection with *C. parvum*. Because of its closer approximation to the human intestinal morphologic and physiologic environment, the low-shear microgravity cell-culture system may prove to be a significant tool in both the assessment of human intestinal epithelial-cell response to infection and the evaluation of potential targets for protective and therapeutic interventions in cryptosporidiosis.

Acknowledgment

We thank the Advanced Microscopy Facility, the Research Histology Core, and the Digestive Health Research Center Morphology/Imaging Core of the University of Virginia for technical assistance.

References

- Adams RB, Guerrant RL, Zu S, Fang G, Roche JK. *Cryptosporidium parvum* infection of intestinal epithelium: morphologic and functional studies in an in vitro model. *J Infect Dis* **1994**; 169:170–7.
- Griffiths JK, Moore R, Dooley S, Keusch GT, Tzipori S. *Cryptosporidium parvum* infection of Caco-2 cell monolayers induces an apical monolayer defect, selectively increases transmonolayer permeability, and causes epithelial cell death. *Infect Immun* **1994**; 62:4506–14.
- Upton SJ, Tilley M, Brillhart DB. Comparative development of *Cryptosporidium parvum* (Apicomplexa) in 11 continuous host cell lines. *FEMS Microbiol Lett* **1994**; 118:233–6.
- Laurent F, McCole D, Eckmann L, Kagnoff MF. Pathogenesis of *Cryptosporidium parvum* infection. *Microbes Infect* **1999**; 1:141–8.
- Seydel KB, Zhang T, Champion GA, et al. *Cryptosporidium parvum* infection of human intestinal xenografts in SCID mice induces production of human tumor necrosis factor alpha and interleukin-8. *Infect Immun* **1998**; 66:2379–82.
- Argenzio RA, Lecce J, Powell DW. Prostanoids inhibit intestinal NaCl absorption in experimental porcine cryptosporidiosis. *Gastroenterology* **1993**; 104:440–7.
- Argenzio RA, Armstrong M, Rhoads JM. Role of the enteric nervous system in piglet cryptosporidiosis. *J Pharmacol Exp Ther* **1996**; 279:1109–15.
- Abrahamsen MS, Lancto CA, Walcheck B, Layton W, Jutila MA. Localization of alpha/beta and gamma/delta T lymphocytes in *Cryptosporidium parvum*-infected tissues in naive and immune calves. *Infect Immun* **1997**; 65:2428–33.
- Unsworth BR, Lelkes PI. Growing tissues in microgravity. *Nat Med* **1998**; 4:901–7.
- Hammond TG, Hammond JM. Optimized suspension culture: the rotating-wall vessel. *Am J Physiol Renal Physiol* **2001**; 281:F12–25.
- Goodwin TJ, Jessup JM, Wolf DA. Morphologic differentiation of colon carcinoma cell lines HT-29 and HT-29KM in rotating-wall vessels. *In Vitro Cell Dev Biol* **1992**; 28A:47–60.
- Goodwin TJ, Schroeder WF, Wolf DA, Moyer MP. Rotating-wall vessel coculture of small intestine as a prelude to tissue modeling: aspects of simulated microgravity. *Proc Soc Exp Biol Med* **1993**; 202:181–92.
- Carvalho HM, Teel LD, Goping G, O'Brien AD. A three-dimensional tissue culture model for the study of attachment and effacement lesion formation by enteropathogenic and enterohaemorrhagic *Escherichia coli*. *Cell Microbiol* **2005**; 7:1771–81.

14. Carterson AJ, Honer zu BK, Ott CM, et al. A549 lung epithelial cells grown as three-dimensional aggregates: alternative tissue culture model for *Pseudomonas aeruginosa* pathogenesis. *Infect Immun* **2005**; 73:1129–40.
15. Honer zu BK, Ramamurthy R, Ott CM, et al. Three-dimensional organotypic models of human colonic epithelium to study the early stages of enteric salmonellosis. *Microbes Infect* **2006**; 8:1813–25.
16. Nickerson CA, Goodwin TJ, Terlonge J, et al. Three-dimensional tissue assemblies: novel models for the study of *Salmonella enterica* serovar *Typhimurium* pathogenesis. *Infect Immun* **2001**; 69:7106–20.
17. Parr JB, Sevilleja JE, Amidou S, et al. Detection and quantification of *Cryptosporidium* in HCT-8 cells and human fecal specimens using real-time polymerase chain reaction. *Am J Trop Med Hyg* **2007**; 76:938–42.
18. Goodgame RW, Kimball K, Ou CN, et al. Intestinal function and injury in acquired immunodeficiency syndrome-related cryptosporidiosis. *Gastroenterology* **1995**; 108:1075–82.
19. Lima AA, Silva TM, Gifoni AM, et al. Mucosal injury and disruption of intestinal barrier function in HIV-infected individuals with and without diarrhea and cryptosporidiosis in northeast Brazil. *Am J Gastroenterol* **1997**; 92:1861–6.
20. Genta RM, Chappell CL, White AC Jr, Kimball KT, Goodgame RW. Duodenal morphology and intensity of infection in AIDS-related intestinal cryptosporidiosis. *Gastroenterology* **1993**; 105:1769–75.
21. Lumadue JA, Manabe YC, Moore RD, Belitsos PC, Sears CL, Clark DP. A clinicopathologic analysis of AIDS-related cryptosporidiosis. *AIDS* **1998**; 12:2459–66.
22. Orenstein JM. Cryptosporidiosis. In: Connor DH, Chandler FW, Manz HJ, Schwartz DA, Lack EE, eds. *Pathology of infectious diseases*. Stamford, CT: Appleton & Lange, **1997**:1147–68.
23. Dabos KJ, Nelson LJ, Bradnock TJ, et al. The simulated microgravity environment maintains key metabolic functions and promotes aggregation of primary porcine hepatocytes. *Biochim Biophys Acta* **2001**; 1526:119–30.
24. Margolis LB, Fitzgerald W, Glushakova S, et al. Lymphocyte trafficking and HIV infection of human lymphoid tissue in a rotating wall vessel bioreactor. *AIDS Res Hum Retroviruses* **1997**; 13:1411–20.
25. Beeson JG, Rogerson SJ, Cooke BM, et al. Adhesion of *Plasmodium falciparum*-infected erythrocytes to hyaluronic acid in placental malaria. *Nat Med* **2000**; 6(1):86–90.
26. Guo P, Weinstein AM, Weinbaum S. A hydrodynamic mechanosensory hypothesis for brush border microvilli. *Am J Physiol Renal Physiol* **2000**; 279:F698–712.
27. Stock UA, Vacanti JP. Cardiovascular physiology during fetal development and implications for tissue engineering. *Tissue Eng* **2001**; 7:1–7.
28. Cai Z, Xin J, Pollock DM, Pollock JS. Shear stress-mediated NO production in inner medullary collecting duct cells. *Am J Physiol Renal Physiol* **2000**; 279:F270–4.
29. Nickerson CA, Ott CM, Wilson JW, et al. Low-shear modeled microgravity: a global environmental regulatory signal affecting bacterial gene expression, physiology, and pathogenesis. *J Microbiol Methods* **2003**; 54:1–11.
30. Hammond TG, Benes E, O'Reilly KC, et al. Mechanical culture conditions effect gene expression: gravity-induced changes on the space shuttle. *Physiol Genomics* **2000**; 3:163–73.
31. Johanson K, Allen PL, Lewis F, Cubano LA, Hyman LE, Hammond TG. *Saccharomyces cerevisiae* gene expression changes during rotating wall vessel suspension culture. *J Appl Physiol* **2002**; 93:2171–80.
32. Nickerson CA, Ott CM, Wilson JW, Ramamurthy R, Pierson DL. Microbial responses to microgravity and other low-shear environments. *Microbiol Mol Biol Rev* **2004**; 68:345–61.